Cost-effective GNSS as a tool for monitoring volcanic deformation

A case study on Saba in the Lesser Antilles

Krietemeyer, Andreas; van Dalfsen, Elske

DOI
10.1016/j.jvolgeores.2024.108263

Publication date
2025

Document Version
Final published version

Published in
Journal of Volcanology and Geothermal Research

Journal of Volcanology and Geothermal Research 459 (2025) 108263

Contents lists available at ScienceDirect

Journal of Volcanology and Geothermal Research

journal homepage: www.journals.elsevier.com/journal-of-volcanology-and-geothermal-research

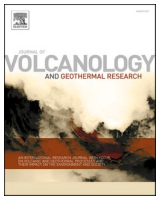

Cost-effective GNSS as a tool for monitoring volcanic deformation: A case study on Saba in the Lesser Antilles

Andreas Krietemeyer [a,*], Elske van Dalfsen [a,b]

[a] Royal Netherlands Meteorological Institute (KNMI), R&D Seismology and Acoustics, Utrechtseweg 297, De Bilt 3731GA, the Netherlands
[b] Delft University of Technology (TU Delft), Geoscience & Remote Sensing, Stevinweg 1, Delft 2628CN, the Netherlands

ARTICLE INFO

Keywords:
GNSS
Cost-effective
Saba
Volcano monitoring
Deformation monitoring
Lesser Antilles

ABSTRACT

We present the design and positioning results of four cost-effective Global Navigation Satellite System (GNSS) units deployed on Saba, Caribbean Netherlands. Despite harsh environmental conditions and initial prototyping challenges the units function well. Each unit costs less than €1.000 and integrates solar charging capabilities, data logging and data transmission via the introduced 4G extension. The positioning performance of the cost-effective units is comparable to those of conventional permanent GNSS stations on the island, with standard deviations in the horizontal and vertical components within 2–4 mm and 6–9 mm, respectively. The cost-effective units can be used to expand existing GNSS monitoring networks or to build stand-alone networks in budget-constrained environments. Their rapid deployment solution makes them suitable for hazardous applications. Future improvements to the current Printed Circuit Board (PCB) design, implementing the presented changes, are anticipated. The schematics of the PCBs, material lists, and software are made available to the community.

1. Introduction

With geodetic observations highly accurate spatial and temporal changes of the Earth's system can be characterized. One technique used for geodetic monitoring is Global Navigation Satellite System (GNSS) measurements. The value of GNSS measurements is evident from the diverse applications including the use of precise timing and positioning (Leick et al., 2015), monitoring of atmospheric properties within the ionosphere and troposphere Jakowski et al. (2002), Bevis et al. (1992), as well as the monitoring of phenomena such as landslides (Gili et al., 2000), crustal deformations (Wilkinson et al., 2023), tectonic plate movements (Kreemer et al., 2014), and seismological activities (Nie et al., 2016). In volcanology, GNSS measurements are used to detect ground deformations and yield insight into magmatic systems or mechanics of caldera formations (Anderson and Johanson (2022); Aoki (2024); Segall et al. (2019)). They can also reveal displacements consistent with dike intrusions (e.g., Parks et al. (2023)) or volcanic/tectonic faulting (Dumont et al. (2022); Poland et al. (2017)) and hydrothermal activity (Bonforte et al. (2024)).

Using GNSS, ground position precision down to the centimeter level or less can be reached even for real-time applications (Teunissen and Montenbruck, 2017). Traditionally this is achieved using expensive, geodetic-grade GNSS receivers along with high-precision antennas. For classical GNSS processing applications, the data is then processed either over baselines between a) two stations (single baseline), b) multiple baselines between multiple GNSS stations (network processing) or c) in a stand-alone mode where data from each GNSS station is processed individually (Precise Point Positioning [PPP]). For the latter, observations tracked from at least two frequencies are required (Zumberge et al., 1997).

Cost-effective GNSS technology has been on the market for about a decade starting with single-frequency GNSS receivers. The use of these receivers in combination with a cost-effective GNSS antenna is challenging because of e.g., constraints on the number of concurrently tracked channels, errors caused by the ionosphere and generally less precise antenna performance. Despite these limitations, these receivers facilitate outcomes that can be deemed comparable to those obtained using geodetic-grade equipment (Marut et al. (2024); Krietemeyer et al. (2020); Garrido-Carretero et al. (2019)). This generated an interest in scientific communities using this equipment for precise applications (e.g., suggested for volcano monitoring by Saunders et al. (2023) or Wilkinson et al. (2023)). The release of cost-efficient dual-frequency

* Corresponding author.
E-mail addresses: andreas.krietemeyer@knmi.nl (A. Krietemeyer), dalfsen@knmi.nl (E. van Dalfsen).

https://doi.org/10.1016/j.jvolgeores.2024.108263
Received 26 September 2024; Received in revised form 10 December 2024; Accepted 19 December 2024
Available online 27 December 2024

receivers a few years ago, spurred a further increase in use, as the data processing became easier. With dual-frequency data every station can be processed individually, using PPP processing.

Most studies conducted with cost-efficient dual-frequency receivers use the u-blox ZED-F9P GNSS receiver (available for about 200€) for which the receiver noise is reported to be in the sub-mm level (Hamza et al., 2021). Several studies compared the positioning performance of the ZED-F9P receiver with different antennas ranging from low-cost to geodetic-grade (Janos et al. (2022); Wielgocka et al. (2021); Tunini et al. (2022), Hohensinn et al. (2022); Krietemeyer et al. (2022); Marut et al. (2024)). They report a positioning accuracy from mm to cm, depending on the receiving antenna and processing application and suggest that the main limitation of a cost-effective setup is the quality of the receiving antenna. This means that to achieve precise results, the use of a high quality antenna (with a nearly equal antenna phase pattern in all directions) or calibration of the receiving antenna (Krietemeyer et al., 2020) is essential. Marut et al. (2024) show an assessment of the quality of raw GNSS signals obtained with the ZED-F9P module and a range of cost-efficient antennas. There are also other manufacturers on the market that produce cost-efficient GNSS modules. The most prominent one is the Mosaic-X5 receiver from Septentrio used in a recent study by Vidal et al. (2024). Though the sole hardware cost of the receiver itself is about three times compared to the ZED-F9P, it can still be considered as cost-efficient because the price is far below the cost of a conventional GNSS receiver.

Even though volcano geodesy is seen as one of the major pillars of volcano surveillance (Poland and de Zeeuw-van Dalfsen, 2021) worldwide less than half of the Holocene volcanoes are monitored with a ground-based deformation network (Widiwijayanti et al., 2024). The high cost of equipment is often a limiting factor in the deployment of a ground-based volcano deformation monitoring network, especially in developing nations, where volcanic hazard can be very high. The use of alternative cost-effective equipment can in such cases be highly advantageous. Therefore, we investigate the use of cost-effective dual-frequency GNSS units for deformation monitoring on the volcanic island of Saba in the Caribbean Netherlands.

2. Case study on Saba

The island of Saba (Northernmost island in the Lesser Antilles Arc, Fig. 1) in the Caribbean Netherlands is home to the active but quiescent stratovolcano, Mt. Scenery, with one charcoal sample dating the last eruption to around 1640 CE (Roobol and Smith, 2004). KNMI operates a comprehensive multi-sensor geophysical monitoring network (Fig. 2) on Saba. Currently, the monitoring network includes four permanent GNSS stations (SABY, SABA, SABN, and SABP) and five broadband seismometers (SABY, SABA, SABN, SABW and SABQ). SABN and SABP operate as off-grid stations, powered by solar panels, with data transmission facilitated by a mobile 4G network (SABP) and satellite communication via a VSAT dish (SABN). The seismic stations are integrated into the seismic Netherlands Antilles (NA) network (Sleeman and de Zeeuw-van Dalfsen, 2022). Additionally, three permanent temperature probes are deployed: i) near the hotspring opposite Green Island, ii) at the abandoned sulfur mine and iii) in the Green Gut. The permanent GNSS stations (De Zeeuw-van Dalfsen and Sleeman, 2018) are strategically located around the volcano with the aim to detect potential deformations resulting from moving or accumulating magma in the subsurface.

To complement the existing permanent GNSS monitoring network, and to verify the feasibility of using cost-effective GNSS for volcano monitoring, four experimental cost-effective GNSS units were installed in February 2022 (Fig. 2 and Fig. 3). SC00 is positioned at the site of the future harbor, SC01 is in Windwardside, and SC02 is atop Mt. Scenery. For evaluation purposes, SC03 is co-located with the permanent GNSS station SABP.

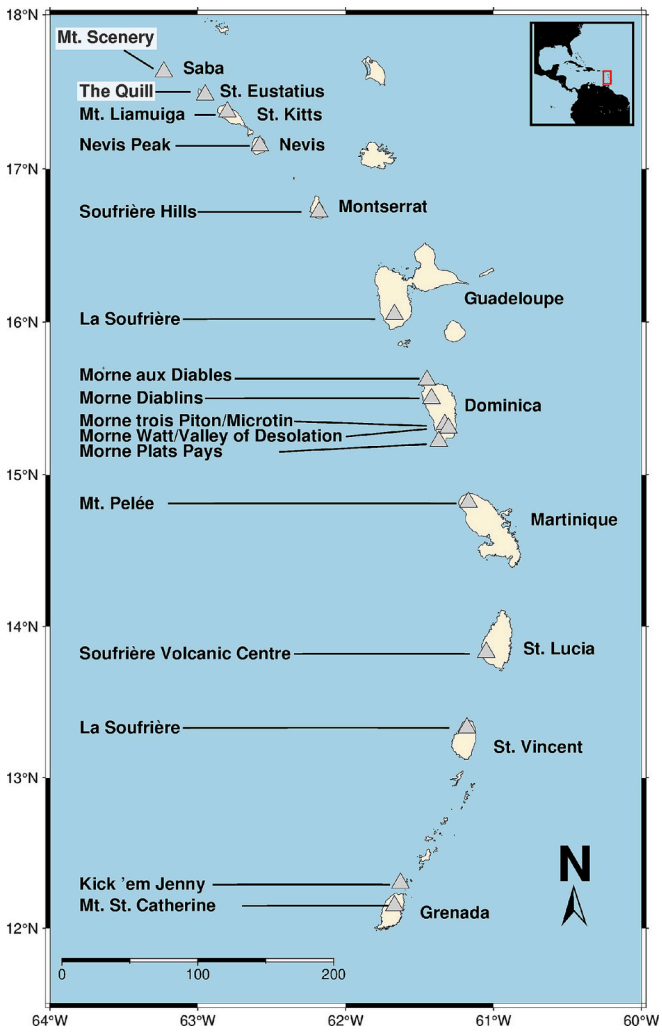

Fig. 1. The islands of the Lesser Antilles volcanic arc with their names shown on the right. Saba is the northernmost island. Grey triangles indicate the location of active volcanoes with their names indicated on the left. The inset shows the geographical location of the arc with a red bounding box. (For interpretation of the references to colour in this figure legend, the reader is referred to the web version of this article.)

3. Cost-effective GNSS unit design

For our installations, we choose to use the Ardusimple "Survey GNSS Multiband antenna" as GNSS antenna and the u-blox ZED F9P as GNSS receiver to balance costs versus data quality. Both are capable of tracking dual-frequency GNSS data while the overall setup costs remain below €1.000 per unit. This is a fraction of the equipment cost of a permanent conventional GNSS station, which quickly exceeds €10.000. One limitation of the GPS L2 signals recorded by the ZED-F9P receiver is that it only tracks signals on L2C. These signals are only available on newer generation GPS satellites. This slightly limits the number of satellites with simultaneous dual-frequency signals available. Due to the high total number of available satellites, this drawback however has marginal implications.

Originally, the prototype used in this work was developed as part of a Ph.D. initiative within the BRIGAID (BRIGAID, 2020) and TWIGA (TWIGA, 2021) projects. In its early stages, the prototype comprised a Raspberry Pi Zero, a power bank, the Ardusimple u-blox ZED-F9P receiver, and the u-blox ANN-MB-00 patch antenna. The prototype development commenced at TU Delft, and subsequent testing took place in close proximity to the International GNSS Service (IGS) station in

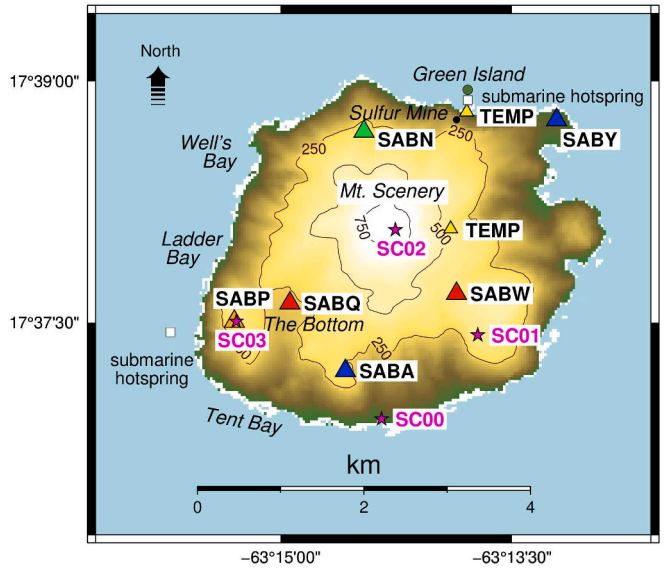

Fig. 2. The current monitoring network on Saba consisting of: permanent GNSS stations co-located with broadband seismometers (blue triangles), a permanent off-grid GNSS station (orange triangle), a permanent off-grid GNSS station co-located with a broadband seismometer (green triangle), broadband seismometers (red triangles) and temperature sensors (yellow triangles). The cost-effective units are depicted using purple stars. (For interpretation of the references to colour in this figure legend, the reader is referred to the web version of this article.)

Delft, which served as a reference point. Studies revealed that the setup could yield results of similar quality to geodetic-grade configurations (Krietemeyer et al., 2020). With the implementation of a locally performed antenna calibration, the prototype achieved high-quality Zenith Total Delay (ZTD) results with a Root Mean Square (RMS) of 4 mm. Furthermore, improvements were observed in Real-Time Kinematic (RTK) and static Precise Point Positioning (PPP) results, leading to a reduction in biases and a lower standard deviation of the estimates.

The prototype was further refined and developed into a stand-alone unit by adding solar panels, solar charge controllers, and lithium-ion batteries (Verweij, 2020), Fig. 4 A and C). Also, all components were either integrated or designed to be plugged into the Printed Circuit Board (PCB) of the system (Fig. 4 B). The solar charging capacity was originally designed for deployment in sun-rich countries in the Global South. It consists of a 20Wp (watt-peak) solar panel and has an overall maximum battery capacity of 140 Wh. To quantify the power consumption, we measured the current of the components with a multimeter and converted it to power (Watt). The Raspberry with GNSS module and antenna connected consumes around 1.75 Wh. The 4G module extension approximately 0.7 Wh. Due to the uncertainty of the measurement, we indicate the total consumption at about 3 Wh. With fully charged batteries, the system can therefore run up to a maximum of two days without power input generated by the solar panel. The PCB schemes and a comprehensive list of all incorporated components are available for download on the GitHub page (Verweij, 2023). One notable advantage of the cost-effective unit design is the ease of swapping components, both hardware and electrical.

High quality positioning and tropospheric results could be achieved with the u-blox ANN-MB-00 antenna in combination with an antenna calibration (Krietemeyer et al., 2020), (Krietemeyer et al., 2022). This antenna was included in the original design. In the prototype used in this study, we replace the ANN-MB-00 antenna with the Ardusimple "Survey GNSS Multiband antenna". The positioning accuracy of this antenna, even without antenna calibration, is on a high level (see also Marut et al. (2024)). With respect to the data transmission, the original prototype was limited to sending data via a 2G connection and the PCB design revealed a wiring fault, impeding the delivery of sufficient power to reach the 2G modem (Fig. 4 C). To overcome the wiring limitation, an additional circuit was implemented. This newly added circuit is solely responsible for the mobile network connection. We now use a 4G module (Fig. 4 D) featuring global frequency band coverage (SIM7600G). The software of our latest distribution has been tailored to support internet connection via the 4G connection. Currently, the system can transmit files to a server on a daily basis, and real-time

Fig. 3. Photos of the four cost-effective units installed on Saba: SC00 is at the location of the future harbor, SC01 is in Windwardside and SC02 is on top of Mt. Scenery. SC03 is co-located with permanent GNSS station SABP.

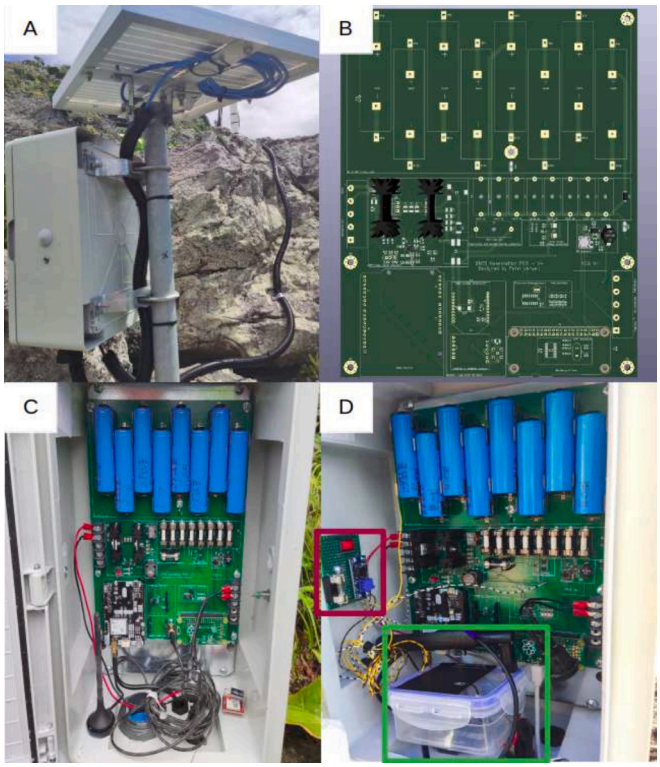

Fig. 4. Technical components of the cost-effective GNSS units. Top left corner (A) shows the electrical box with pole, solar panel and metal mounting brackets. Top right (B) shows the PCB of the original design as available via GitHub. Bottom left (C) shows the installed inside of the electrical box without modifications. Bottom right (D) shows the modifications for the data connection highlighted in red (additional power circuit) and green (4G unit) rectangles. (For interpretation of the references to colour in this figure legend, the reader is referred to the web version of this article.)

streaming data with RTCM3 (Radio Technology Commission for Maritime Services) messages can be configured. Due to the relatively high cost of data transmission (~$20/month) only one site (SC00) is outfitted with a mobile network connection. However, all stations log 15-second data locally, with sufficient storage capacity for at least two years. Data are manually retrieved during routine visits to the island. A standard software package for using the described unit and modifications has been mirrored to an SD card image, available at 4TU (Krietemeyer and van Dalfsen, 2024). It can be flashed to SD cards sizes 8GB or larger.

Solutions for software errors, which were identified and remedied throughout the experiment, are fully incorporated into the current system. Another issue involved the steel door hinges of the electrical box, which extensively corroded. These hinges were replaced with carbon sticks in October 2023. Following the modifications above, the system operates independently with remote access possibilities and automatic data transmission. However, a comprehensive review of the electrical components is recommended to incorporate these modifications into the PCB design. Given that the system was originally designed for deployment in countries with high sun-hours throughout the year, it currently relies solely on solar power. Introducing the capability for the system to also operate on wind power would be advantageous. Improvements of the software would be beneficial to enhance robustness of the system and also eliminate manual configuration steps which are currently necessary to configure the u-blox receiver to log raw data in the specified logging interval.

Regardless of the type of measurement device installed in the field, the exposure to the environment must be taken into consideration. Particularly challenging in the Caribbean are high winds, intense UV radiation, and salty sea spray. The cost-effective units are therefore designed with robustness in mind, utilizing materials such as high grade stainless steel, aluminum, and reinforced brackets for mounting the electrical box and accompanied solar panel. Two different installation types were used for the prototype installations on Saba. The first design integrates the antenna, instrument box, and solar panel onto a single pole (Fig. 5a) and was implemented at the location of the future harbor (SC00). The second design (Fig. 5b) consists of an antenna rod installed detached from the instrument and solar panel pole. This separated design was installed at the remaining sites (SC01, SC02, and SC03). Both designs use quick-dry chemical two-component mortar to fix the bolts to the ground.

Installation time does not significantly differ between the two designs. Depending on technical affinity and routine, both installations require approximately one hour to drill holes and install the materials, even for non-technical personnel. The separated design offers the advantage of placing the antenna detached from the instrument box. This could potentially be on top of an exposed boulder, while locating the solar panel and instrument box in a more secure location. Additionally, the footprint of the installed poles (10x10cm) is smaller, using less heavy material. This design also minimizes potential reflections from the solar panel to the antenna phase pattern. Depending on the chosen antenna cable, the antenna can be placed at several metres distance to the instrument box. In contrast, the combined solution may be more robust, featuring a thicker pole and a larger footprint (20x20cm). With approximately one metre pole height, the antenna is also higher, enabling it to stay above growing vegetation. With all components in one place, and due to the nature of placing a GNSS antenna in preferably open sky conditions, it is more exposed to the elements. Because of the advantages of separating the antenna from the instrument box, we chose this design for three out of four locations. Wherever possible, UV-resistant plastic cable ducts protect the antenna cable and industrial lubricant is used to shield the connectors.

4. Data processing

Data retrieval of the cost-effective units is achieved either by manually extracting the data in the field from the SD card or by downloading it from the server were they are send to. The binary UBX file types are organized into hourly files and subsequently merged into daily RINEX3 files using RTKLIB's convbin (Takasu, 2013) software. These RINEX files are then processed to obtain the station's daily coordinates.

The data is processed either in a network solution (forming baselines between receivers defined in the network) or in PPP. With PPP, each station is processed individually. The downside is that the noise in the data is increased by a factor of 3, making good antenna performance and site selection more important. Table 1 shows an overview of the used processing methods.

We process the data of the GNSS stations on Saba in five different ways: BSW-PN: The routine, operational, processing of the KNMI permanent network (including stations on both Saba and St. Eustatius) using a Bernese 5.4 network solution; NRCAN-PPP: An NRCan (Banville et al., 2021) online PPP solution; BSW-PPP: A PPP solution (Bernese 5.4); BSW-PN+CE: A network solution (Bernese 5.4) of our entire GNSS network (including cost-effective and permanent KNMI GNSS sites on Saba and St. Eustatius); and BSW-CE: A network solution (Bernese 5.4) of our cost-effective units excluding the permanent KNMI GNSS sites. The errors reported by the Bernese processing engine of all processing solutions of each station and day are typically below or around 1 mm. High outliers (σ reported >3 mm) are removed from the data. All network solutions use the same external reference sites distributed across the Caribbean and North- and South America (Appendix A.3). The data for these sites is obtained from either the Crustal Dynamics Data Information System (CDDIS) or from the EarthScope archive. The network solutions BSW-PN, BSW-PN+CE and BSW-CE use GPS, GLONASS and Galileo satellites. To include Galileo observations in the cost-

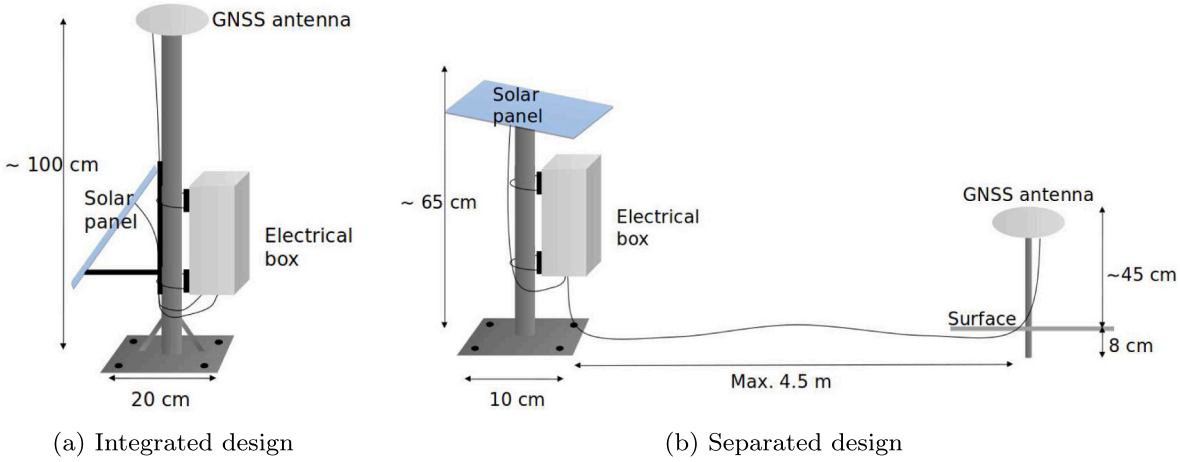

Fig. 5. Two installation designs used on Saba. An integrated design (left) and a separated version (right).

Table 1
Overview of used processing strategies. The entries in the abbreviation column (Abbr.) are used in the text to identify the processing strategy. Bernese solutions are consistent with the IGS20 reference frame. NRCan PPP results switched on 27 November 2022 to IGS20.

Abbr.	Processing Engine	Remarks
BSW-PN	Bernese 5.4 Network	Only permanent GNSS, 3° cutoff GPS,GLO,GAL,
NRCAN-PPP	NRCan PPP	Standalone, 7.5° cutoff GPS,GLO
BSW-PPP	Bernese 5.4 PPP	Standalone, 3° cutoff GPS(+GLO,GAL)
BSW-PN+CE	Bernese 5.4 Network	All stations, 3° cutoff GPS,GLO,GAL
BSW-CE	Bernese 5.4 Network	Only cost-effective units, 3° cutoff GPS,GLO,GAL

effective units processing BSW-PPP, BSW-PN+CE and BSW-CE, the Galileo E5b signal (L7X in RINEX notation) is used (instead of the E5a signal). The 3° cutoff angle is the default setting for the Bernese processing. All Bernese solutions use precise orbit and clock data from the Center for Orbit Determination in Europe (CODE). The NRCAN-PPP solution uses a non-changeable cutoff angle of 7.5 degrees.

The Processing strategies are chosen to investigate applicability and performance of cost-effective units to be used 1) as a standalone deformation monitoring network or 2) to densify an existing GNSS network. The standalone solutions are calculated using solely the newly installed cost-effective units on the island. These are the PPP solutions NRCAN-PPP and BSW-PPP. The network solution BSW-CE uses the external reference sites (Appendix A.3) and the cost-effective GNSS units. Densifying the existing GNSS network on the island is investigated using processing strategies BSW-PN+CE.

Bernese and NRCan allow for fixing the ambiguities to integer values. With NRCan, only GPS is fixed to integer and GLONASS observations remain float. In Bernese 5.4, GPS and Galileo ambiguities can be resolved to integer. However, this requires to apply so-called observable-specific signal biases. These biases from the CODE analysis center are not available for the Galileo E5b signals. Our Bernese PPP solutions from the cost-effective units therefore only use GPS satellites for the fixed ambiguity resolution. The processing of permanent GNSS stations with PPP additionally uses Galileo satellites, as they track data on the

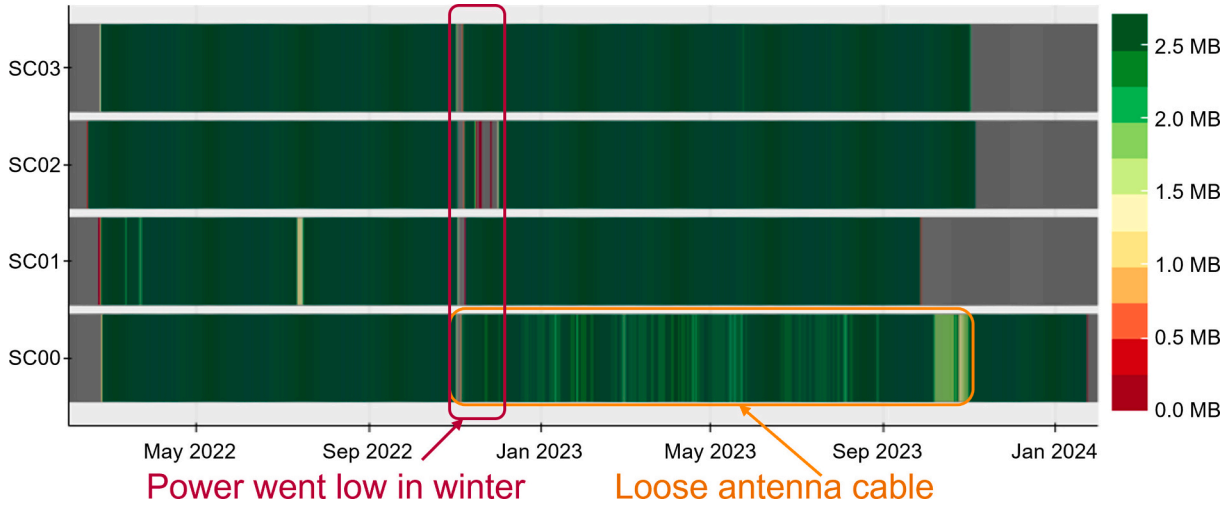

Fig. 6. Data availability of the units for 2022–2023 whereby dark green indicates a file size above 2.5 MB. Lighter colors depict partial data loss, red almost empty files and grey means no files were archived. (For interpretation of the references to colour in this figure legend, the reader is referred to the web version of this article.)

Table 2
Inventory of the cost-effective unit station availability. The arbitrary file size threshold of a file considered full is set to 2.5 MB.

Station	Start-End dates	#Days	%	#Days>2.5 MB	%
SC00	2022-02-23–2023-12-31	675/677	99.7 %	483/677	71.3 %
SC01	2022-02-21–2023-11-01	580/619	93.7 %	566/619	91.4 %
SC02	2022-02-13–2023-11-04	615/630	97.6 %	605/630	96.0 %
SC03	2022-02-22–2023-11-01	615/618	99.5 %	610/618	98.7 %

E5a frequency for which these biases are provided.

Atmosphere and ocean loading effects are removed from all processing runs. Given that the utilized antennas of the cost-effective units are uncalibrated, an empty antenna pattern was appended to the Bernese antenna calibration files.

The obtained positions (XYZ, Earth Centered, Earth Fixed - ECEF) and geographic coordinates are transformed to a local coordinate system originating at the location of the first epoch of each antenna. Trend parameters were obtained by using least squares estimation using the following formula:.

$$y(t) = a + b^{*}t + A^{*}cos(f^{*}t + phi) \quad (1)$$

Where a is the intercept, b the slope, A the amplitude, f the frequency (fixed to an annual component) and phi the phase shift. We estimate the parameters a, b, A and phi using a least squares estimation.

5. Runtime

The data availability for all four cost-effective units remained consistently high, with an average availability between 91 % (SC01) and 99 % (SC03) shown in Fig. 6 and Table 2.

All four cost-effective units faced a power outage in November 2022, due to the low number of sun hours. This situation is rare and was not repeated since. Station SC02, situated atop Mt. Scenery, exhibited the highest data gaps, likely attributed to common higher cloud cover on the mountain hampering solar charging and causing power outages. As anticipated, the system autonomously came back online. To address potential winter power shortages in the future, a larger solar panel is recommended. During this period, also the permanent GNSS station SABN relying on solar power, experienced power outages due to the lack of sun hours. Overall, the data availability of the permanent GNSS stations is generally better, averaging to above 99 %. This is not surprising as two of the four permanent stations are connected to a stable power line and only SABN and SABP are running on solar powered batteries.

Between November 2022 and November 2023, station SC00 exhibited reduced data quality due to a loose antenna connector (approx. 71 % files are >2.5 MB), which was replaced in November 2023. This issue resulted in some data being inaccurately tracked by the receiver during this period. Despite this hardware issue, we included the processing results into our analysis as since November 2023 this station is equipped with 4G connection, transmitting data to KNMI on a daily basis.

GNSS unit SC01 has the second lowest data availability of approximately 91 %. This is related to an unexplainable software error on 27 September 2023 (rightmost vertical red line in SC01 row in Fig. 6). Most likely cause is that the device was stuck in a boot loop. After a restart and supplying updated software to the device in November 2023, the device continued recording data. November 2023 was also the last time data was collected offline from the stations SC00, SC01 and SC02. The next data collection is planned in 2024 but will not be considered in this manuscript.

6. Daily positioning results

As outlined in section 4, we processed the GNSS data with a range of different processing methods (Table 1). The positioning estimation is done with daily GNSS files, resulting in one position per day per station. All stations show a movement in the Northeastern direction, aligning with the anticipated Caribbean Plate movement. We refer to these trends as velocities here. Note that we are not focusing on potential deformation on the island, but instead look into the dispersion of the data as a measure to determine the performance of the cost-effective GNSS units in comparison to their conventional counterparts. For this purpose in the further analysis in this paper, station-specific linear and seasonal trends (eq. 1) were removed from the data. Fig. 7 shows the estimated yearly velocities in North, East and up directions using the BSW-PN and BSW-PN+CE processing solutions. The estimated values can also be found in Table B.1 in the appendix. Assuming zero random walk error over long time spans, we estimate their uncertainties (σ_{trend}) for each station by scaling the standard deviations of the residuals by the length of the time series in years. It has to be noted that the time spans used to estimated the velocities (between 389 and 669 days) are short. For tectonic

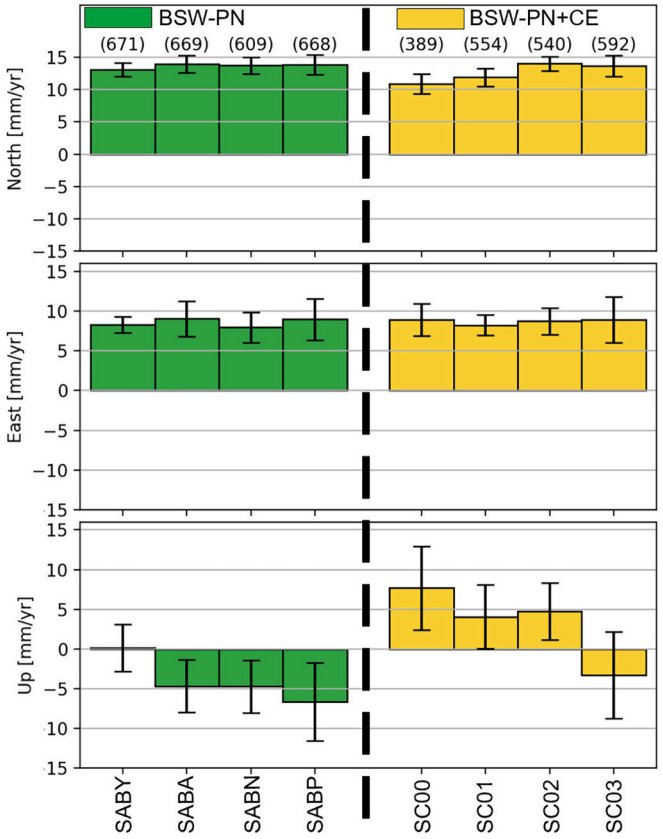

Fig. 7. Estimated velocities in mm/year in North, East and up directions using the BSW-PN (green, left; permanent GNSS stations) and BSW-PN+CE (yellow, right; cost-effective GNSS units) processing solutions. The values in brackets denote the number of days available for obtaining the solutions. The whiskers above each bar denotes the estimated error of the respective velocity. (For interpretation of the references to colour in this figure legend, the reader is referred to the web version of this article.)

interpretation typically 2.5 years of data should be used (Blewitt and Lavallée, 2002).

The estimated velocities in Fig. 7 show the movements of all stations in North, East and up directions. It can be seen that the permanent stations generally have more observation days available compared to the cost-effective units. The reason for this lies in the chosen data period ending on 31 December 2023, as SC01, SC02 and SC03 lack data from November and December due to the last offline data collection in October. However, also removal of data outliers plays a role. The data of SC00 includes only 389 days of data mostly caused by the loose antenna cable.

As for the velocities in North direction, all stations agree reasonably well with each other. Only SC00 and SC01 show a slight difference (between one and two mm). The estimate of SC01 is however within the error range to match the velocity of the remaining stations. All stations agree well in East direction. Only in up direction, the estimates deviate noticeably. The up direction is generally estimated with the highest uncertainty, and thus is the error range also highest.

Assuming constant velocities, the estimates become more accurate for longer time series. The velocity estimates of the whole time series data of our permanent GNSS network (starting in 2018, not shown here) shows a slight downward trend of about 1–2 mm per year for all stations. The results shown here use data of less than two years with a higher uncertainty. This demonstrates the consequences of using shorter time spans for velocity estimations because also the permanent network stations show deviations in the up component, which are not evident when using the full dataset (2018+). It is therefore most likely that a longer time series will improve the velocity estimations, not only for the permanent stations, but also for the cost-effective units.

Plate tectonics is the main driver causing the movement of the stations. For the same reason identified above, we choose not to compare the estimated velocity trends from the cost-effective units to those derived from a plate model. Instead, we evaluate the reliability of the measurements by looking at the scatter of the obtained daily positions to establish whether the units can produce results similar to their conventional GNSS counterparts.

Fig. 8 shows the boxplots of the standard deviations of all GNSS stations on the island using the BSW-PN and BSW-PN+CE processing solutions after removing the station-specific linear and seasonal trends from the data.

The standard deviations (σ) shown in Fig. 8 (and Table C.1 in the appendix) indicate a good agreement between the permanent GNSS stations and the cost-effective GNSS units. Small boxes and whiskers indicate good data quality with crosses depicting single data points outside the range of the whiskers. In horizontal directions, the median σ ranges from 1.8 to 4.8 mm for the permanent stations and 1.8 to 4.9 mm for the cost-effective sites. In vertical direction, the σ is between 5.4 and 9.0 mm for the permanent stations and between 6.0 and 9.7 mm for the cost-effective sites. It is evident that station SABY at the airport performs best based on the obtained residuals. SC01 in Windwardside and SC02 at the top of Mt. Scenery also demonstrate low standard deviations (~2 mm horizontal and ~6 mm vertical) of the residuals and perform very comparable to the permanent GNSS stations. These units are located at the sites with the least obstructions. This observation indicates that the influence of local factors, like visibility of the horizon, unobstructed sky view and least reflections from nearby objects should not be underestimated. Finding a balance between an optimal location with respect to the volcano and the best satellite tracking possibilities can therefore be very challenging. This may result in stations with slightly lower data quality, e.g. site SABP, which still fulfil the goal of volcano monitoring. Compared to the permanent GNSS stations, less data is available for the cost-effective stations to interpret the obtained positions. This is caused by the offline data collection, data outages and outlier removal during processing and particularly evident for unit SC00.

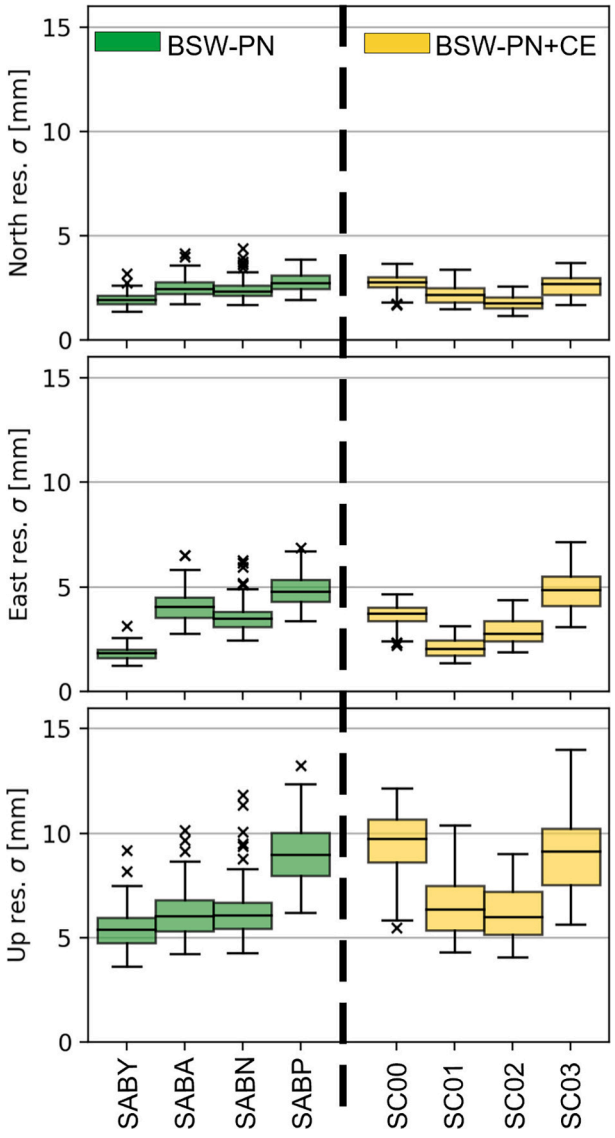

Fig. 8. Boxplots of the estimated standard deviations of the residuals after removing the station-specific linear and seasonal trends from the data using processing solutions BSW-PN (green, left; permanent GNSS stations) and BSW-PN+CE (yellow, right; cost-effective GNSS units). The boxes represent the middle 50 % of the standard deviations, the whiskers the smallest and largest values within 1.5 times the interquartile range and crosses values outside this range. (For interpretation of the references to colour in this figure legend, the reader is referred to the web version of this article.)

We compare the positioning results of the different processing strategies after removing the station-specific linear and seasonal trends (eq. 1) from the data by looking at the Median Absolute Deviation (MAD) in the local coordinate system directions (Fig. 9).

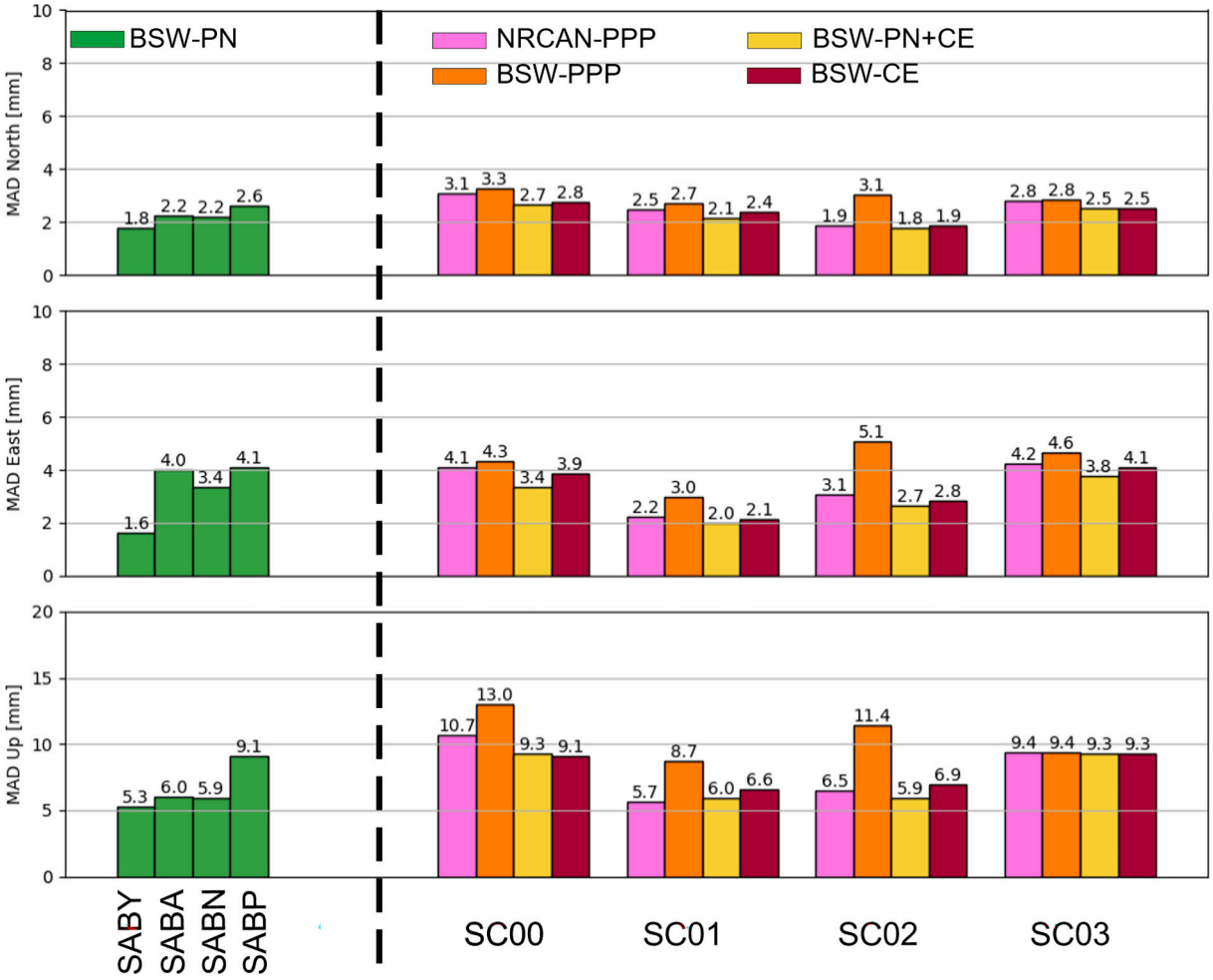

Fig. 9. Comparison of processing strategies. It shows the Median Absolute Deviation (MAD) in North (top), East (middle) and up (bottom) after removal of the station-specific linear and seasonal trends following from eq. 1. Left of the dashed line (green boxes) are the permanent network sites. They are processed using Bernese 5.4 in a network solution (BSW-PN). On the right are the MAD values for the cost effective units in groups of four. Each bar of each unit shows the MAD resulting from the different processing strategies: NRCAN-PPP; BSW-PPP; Bernese 5.4 Network [all sites] - BSW-PN+CE; Bernese 5.4 Network [cost-effective only sites] - BSW-CE. (For interpretation of the references to colour in this figure legend, the reader is referred to the web version of this article.)

$$MAD = 1.4826 \cdot median(|x_i - median(x)|) \quad (2)$$

Where the variables x_i are individual data points and x the entire data set and 1.4826 the scale factor for data which are normally distributed. The MAD is a more outlier resistant measure of the dispersion compared to the standard deviation.

The green columns show the positioning results of the permanent network (BSW-PN) processing. It is evident that station SABY has the lowest residuals and SABP the highest. The deviations are in the mm range (horizontally between 1.6 and 4.1 and vertically between 5.3 and 9.1). Right of the dashed line are the different processing strategy results in pairs of four for each cost-effective unit. Looking across all units one can generally see the lowest errors for station SC01 and highest for SC00 which is expected given the connector issues with SC00. Comparing the different processing strategies, the Bernese PPP processing (BSW-PPP) shows the highest errors. This is rather unsurprising because the processing only takes GPS satellites for the PPP ambiguity resolution into account. The NRCan (NRCAN-PPP) solution however, performed better compared to the Bernese PPP solution (BSW-PPP). This could be because NRCan also takes GLONASS satellites into account and uses a higher elevation cutoff angle. Across all processing schemes, SC03 has mostly higher errors compared to the other stations. This unit is co-located with permanent station SABP where less favourable acquisition conditions were accepted to establish a monitoring side west of the volcano. The influence of local factors on data quality is also seen by looking at the error bars in the up direction of SC01 and SC02, especially for the Bernese PPP processing (BSW-PPP). Because the ionosphere-free linear combination is utilized, the noise introduced by environmental factors is increased. The higher error could be attributed to the vegetation surrounding the antennas. Looking at results from the processing strategy BSW-PN+CE which uses Bernese 5.4 network processing with all stations on the island, the errors in the horizontal directions are between 2 and 4 mm and in vertical direction between 5 and 9 mm. The standalone network processing strategy BSW-CE, using only the cost-effective units on the island, shows a slightly higher but same order of magnitude MAD (maximum of 1 mm in up-direction). This indicates that, looking at data quality, a network of only cost-effective units could be used for volcano monitoring purposes in budget-tight areas.

The Bernese network processing solutions (BSW-PN, BSW-PN+CE, BSW-CE) use a mixture of different ambiguity resolution techniques. In order to form baselines between the external reference GNSS stations and the local GNSS network on Saba, at least one (long) baseline has to be formed between the two. Such a baseline is too long to form only double differences to resolve the integer fixed ambiguities. Instead, an ionosphere-free linear combination is utilized which unfortunately increases the noise in the data. Using observations from the permanent GNSS network on Saba (solutions BSW-PN and BSW-PN+CE) has a clear advantage because the antennas of the permanent GNSS stations are

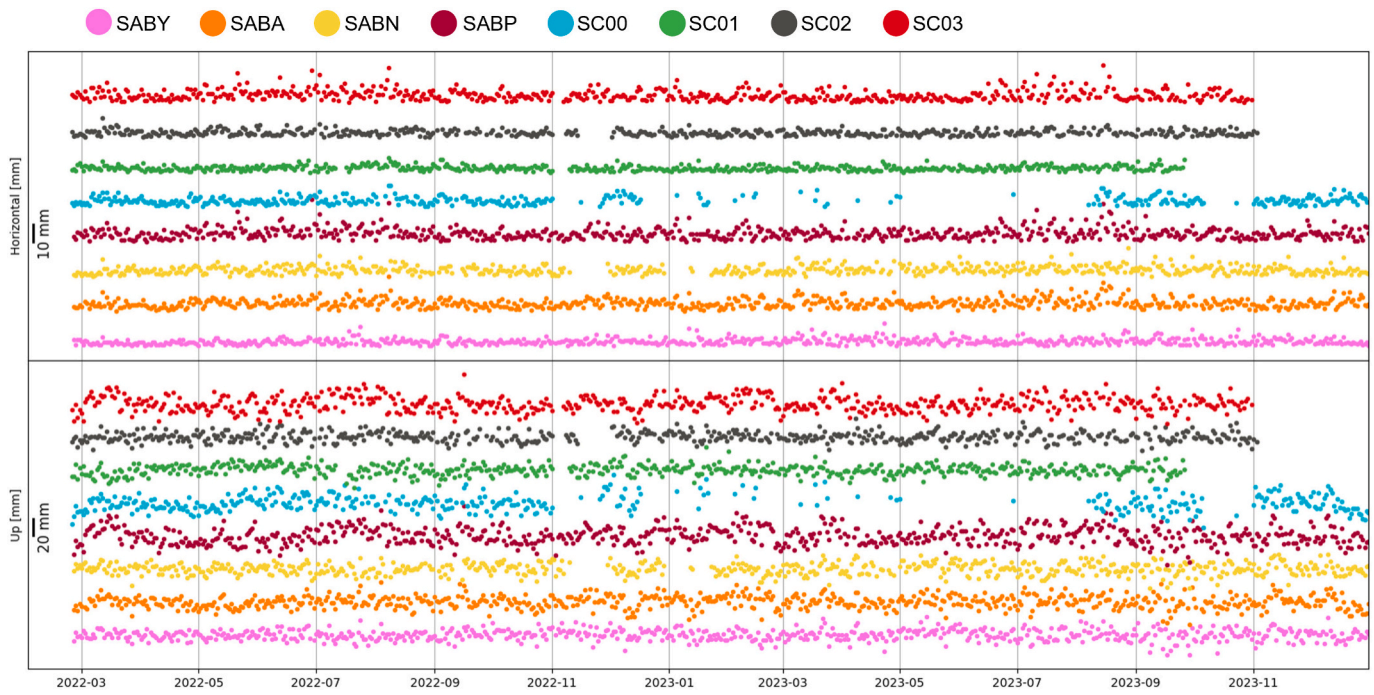

Fig. 10. Horizontal (top) and vertical (bottom) movement after removal of the station-specific linear and seasonal trends. Each colour represents one station. The lowest four lines are the permanent network sites and the top four stations are the cost-effective units. The positions were shifted for visual purposes.

calibrated and the error caused by the receiving antenna phase pattern on the longer baseline can be accounted for. When using only cost-effective units for the network processing (BSW-CE), a higher error compared to the BSW-PN and BSW-PN+CE processing solutions on establishing the longer baseline is expected because of the unknown antenna patterns. The remaining baselines on the island are short baselines where the error caused by the antenna phase pattern is cancelled out if the same antenna pattern is expected for the same antenna model. Calibration of the cost-effective antennas, either performed in the lab or directly in the field (Krietemeyer et al., 2022), may improve the obtained positioning results.

For further analysis, we use the best performing processing strategy BSW-PN+CE which uses the Bernese 5.4 network processing including all stations on the island. We show the horizontal and vertical movement of all stations on the island after removing the station-specific linear and seasonal trends (eq. 1) from the data (Fig. 10).

The top panel shows the horizontal (resulting vector of combining North and East vectors) and the bottom panel the vertical movements for each measurement site. In each panel the lower four lines indicate the permanent network stations and the upper four the cost-effective units. Visual comparison of the cost-effective results with those from the permanent sites reveals only marginal differences in the positioning performance. Evident are multiple monitoring gaps when the solar power could not recharge the batteries and for SC00 (cyan line) the data gaps caused by the processing of data with the loose antenna cable. Stations SC01-SC03 yield no data after November 2023 as this was the last time offline data were collected. Of the cost-effective units, only SC00 displays data after November 2023 because at that location a 4G connection was implemented. Visible is also a period of increased noise between July 2023 and September 2023 in the horizontal direction for data from SC03 (red line) and SABP (dark red line). This is also partly evident for station SABA (orange line). Interestingly, this is followed by a short period in September 2023 of slightly noisier data in the up component across all stations. The underlying cause of this effect remains to be clarified and a closer analysis of the data will be carried out outside the scope of this paper.

7. Positioning comparison of a co-located cost-effective unit to a permanent GNSS station

The cost-effective GNSS unit SC03 is positioned co-located with the permanent GNSS station SABP serving as verification for our analysis. While the true baseline between the antennas is unknown, we evaluated the change over time of the positions. The approximate distance between SC03 and SABP is one metre horizontally and 50 cm vertically.

Fig. 11 shows the direct comparison of the time series in North, East and up components of the permanent station SABP and cost-effective unit SC03 processed using the network processing strategy BSW-PN+CE.

Looking at the daily positioning results and their adjusted standard deviations, the same positioning trend is evident suggesting a similar behaviour of both set-ups. The estimated velocities (Fig. 7, Table B.1) and the standard deviations (Fig. 8, Table C.1) are at a comparable level differing only within the error tolerance. Comparing the MAD of SABP with those of SC03, it can be noted that the observations are rather alike (3–5 mm in horizontal directions and 9 mm in vertical direction). Both, the permanent GNSS station and cost-effective GNSS unit, achieve similar results with respect to their daily positioning performance. Since both sites show similar MADs, the biggest difference lies in the number of days of data that is used in the processing (592 for SC03 and 668 for SABP). Based on data quality alone, cost-effective units could replace more expensive equipment conventionally used for permanent GNSS monitoring. However, data acquisition currently is more robust using conventional GNSS equipment, as is evident from higher data availability. Hence, if sufficient funds are available, conventional GNSS equipment remains the prime choice. If financial constraints are present, or if the area is prone to destruction (by a potential eruption), cost-effective GNSS equipment is deemed a suitable alternative.

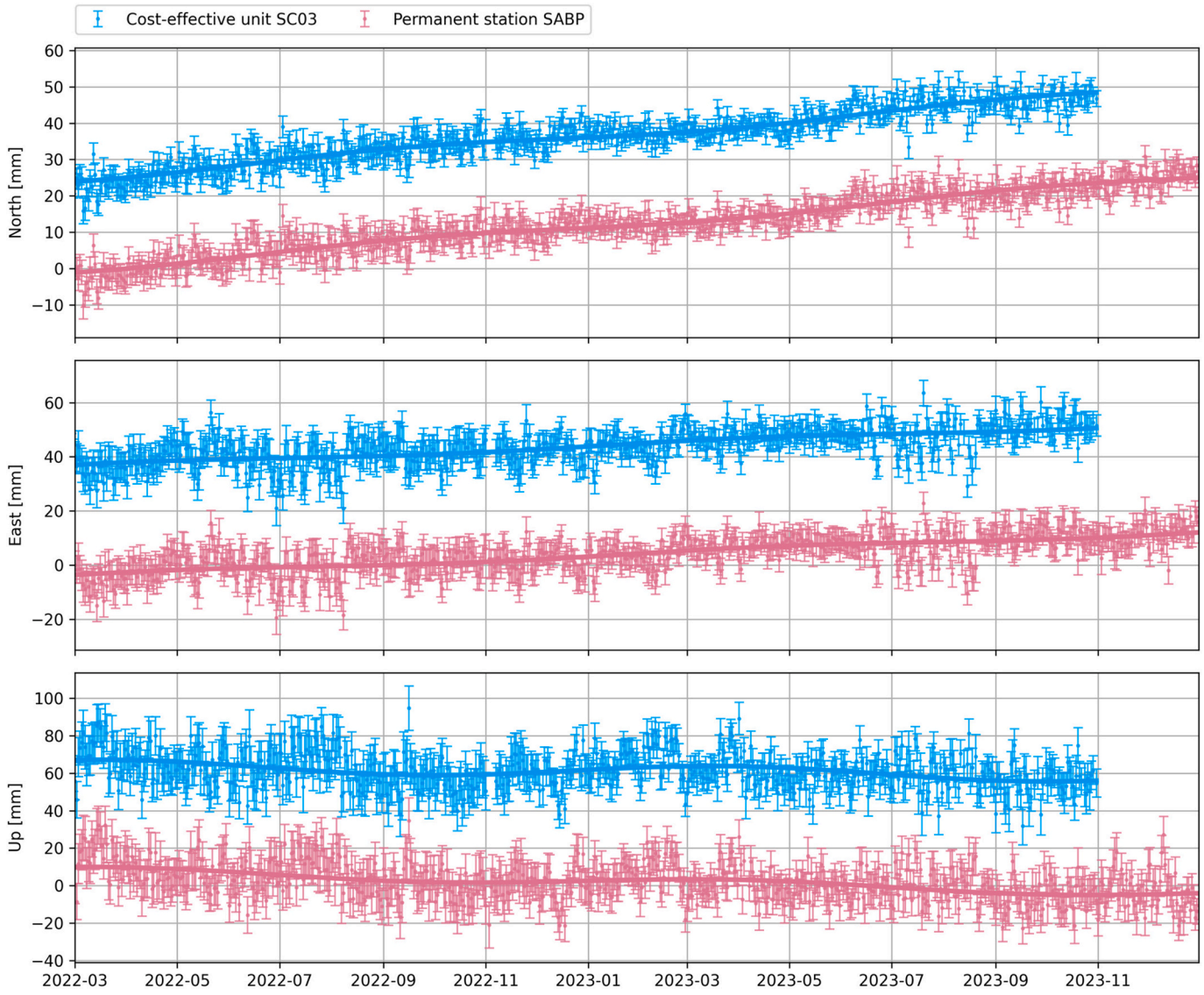

Fig. 11. Comparison of the co-located cost-effective unit SC03 (blue, top line) and permanent GNSS station SABP (red, bottom line). The North (top), East (middle) and up (bottom) components are shown with their respective scaled 1σ error bars and estimated linear and seasonal trends (thick lines). The positions of the cost-effective data are shifted for visual intend. (For interpretation of the references to colour in this figure legend, the reader is referred to the web version of this article.)

8. Conclusions and Outlook

Despite the harsh environmental conditions and initial prototyping issues, four cost-effective GNSS units were successfully deployed on Saba. The units operate independently and are able to log high quality GNSS data. Compared to the permanent GNSS stations the data availability of the cost-effective units is lower. This is partly due to the fact that the majority of the units only record offline data. Disruptions, or erroneous behaviour of the cost-effective units can therefore only be detected from post-analysis and remedied during the next on-site visit. By using the presented 4G extension, data transmission, remote control and continuous monitoring of the unit is possible.

The GNSS data of the cost-effective units can be processed operationally, either as a stand-alone monitoring network or as an expansion of an existing monitoring network. To compare the results, data were processed in stand-alone PPP (NRCAN-PPP, BSW-PPP) or network (BSW-CE) modes and also integrated in an existing network processing scheme (BSW-PN+CE). The quality of the obtained daily processing results depends on the utilized processing strategy. With the best performing processing scheme (BSW-PN+CE), MADs between 2 and 4 mm in the horizontal and 6 to 9 mm in the vertical direction can be achieved for the cost-effective units making them suitable to expand an existing monitoring network. The results from the stand-alone network processing strategy (BSW-CE) are comparable to those of the permanent GNSS network (BSW-PN) and within requirements deemed necessary for volcano monitoring purposes. Furthermore these results are achieved for a fraction of the costs of conventional equipment. With the presented GNSS unit designs, an almost out of the box solution is available. The schematics, list of materials and software necessary to run the units are supplied to the community. The ease of installation enables rapid set-ups in potentially hazardous areas. An improved version of the PCB design, especially implementing the presented changes necessary for 4G connection, is envisioned for the future.

We encourage the deployment of cost-effective GNSS units for volcano monitoring in areas where densification of the existing monitoring network is advantageous or in hazardous environments where rapid installations are important and loss of equipment is deemed viable. Finally, cost-effective GNSS units can be operated as a stand-alone network in budget constrained regions where volcano monitoring is essential.

CRediT authorship contribution statement

Andreas Krietemeyer: Writing – review & editing, Writing – original draft, Visualization, Validation, Software, Methodology, Data curation, Conceptualization. **Elske van Dalfsen:** Writing – review & editing, Writing – original draft, Validation, Methodology, Conceptualization.

Declaration of competing interest

The authors declare that they have no known competing financial interests or personal relationships that could have appeared to influence the work reported in this paper.

Data availability

Data will be made available on request.

Acknowledgements

The authors are thankful to the Public Entity Saba and the Saba Conservation Foundation for their support and for giving permission for the placement of the equipment. We also thank Al Every for allowing installation of SC01.

The authors are particularly grateful to Hans van der Marel for his insightful comments internally reviewing the paper.

Declarations

The software is stored on an SD card image and available via 4TU (Krietemeyer and van Dalfsen, 2024). PCB designs are available on the GitHub repository (Verweij, 2023).

Conceptualization, A.K., E.v.D; methodology, A.K., E.v.D; software, A.K.; validation, A.K., E.v.D; data curation, A.K.; writing—original draft preparation, A.K., E.v.D; writing—review and editing, A.K., E.v.D; visualization, A.K.; All authors have read and agreed to the published version of the manuscript.

The permanent GNSS site SABY is co-owned between KNMI (www.knmi.nl) and Kadaster (www.kadaster.nl).

The work received funding from the European Community's Horizon 2020 Program (2014–2020) under grant agreement No. 776691 (TWIGA) and grant agreement No. 101086209 (TEMBO).

The authors declare no conflict of interest.

Appendix A. Data attribution of external GNSS network stations

Table A.1
Reference sites used for the Bernese network processing.

Station	Data Attribution
ABMF	IGN https://rgp.ign.fr/STATIONS/#ABMF
CRO1	NRAO/JPL https://files.igs.org/pub/station/log/cro1_20230305.log
GODE	GSFC/JPL https://files.igs.org/pub/station/log/gode_20230305.log
KOUG	CNES https://regina.cnes.fr/en/stations/KOUG
KOUR	ESOC https://files.igs.org/pub/station/log/kour_20240117.log
MDO1	MLRS/JPL https://files.igs.org/pub/station/log/mdo1_20230313.log
POVE	IBGE https://files.igs.org/pub/station/log/pove_20230608.log
RDSD	Geomedicion https://files.igs.org/pub/station/log/rdsd_20240129.log
RIOP	IG https://files.igs.org/pub/station/log/riop_20211122.log
SALU	IBGE https://files.igs.org/pub/station/log/salu_20230608.log
SCUB	CENAIS/GFZ https://files.igs.org/pub/station/log/scub_20211116.log
DISD	HoustonNet https://doi.org/10.7283/T5319T64

Table A.2
Abbreviations of A.3.

Abbreviations	
IGN	Institut national de l'information géographique et forestière
NRAO	National Radio Astronomy Observatory
JPL	Jet Propulsion Laboratory
GSFC	Goddard Space Flight Center
CNES	Centre national d'études spatiales
ESOC	European Space Operations Centre
MLRS	McDonald Observatory
IBGE	Instituto Brasileiro de Geografia e Estatística
IG	Instituto Geofísico, Ecuador
CENAIS	Centro Nacional de Investigaciones Sismologicas, Cuba
GFZ	German Research Centre for Geosciences

Appendix B. Estimated velocities

Table B.1
Estimated velocities (Vel.) and their uncertainties (σ_{vel}) in North, East and up directions of the stations in mm per year using available data from 2022-03-01 - 2023-12-31. The permanent GNSS stations SABY, SABA, SABN, SABP are processed with the Permanent Network (BSW-PN) processing scheme and SC00-SC03 with processing scheme BSW-PN+CE) from table 1. The number of days (# days) used for the processing are indicated in the line below the stations names.

	BSW-PN				BSW-PN+CE			
	SABY	SABA	SABN	SABP	SC00	SC01	SC02	SC03
Vel. / # days	671	669	609	668	389	554	540	592
North	13.09	13.93	13.71	13.80	10.86	11.89	13.97	13.66
σ_{vel}	±1.06	±1.35	±1.28	±1.51	±1.51	±1.38	±1.07	±1.62
East	8.31	9.07	7.97	8.97	8.93	8.25	8.74	8.95
σ_{vel}	±1.00	±2.23	±1.92	±2.60	±2.02	±1.29	±1.65	±2.89
up	0.12	−4.68	−4.73	−6.63	7.67	4.04	4.74	−3.32
σ_{vel}	±2.94	±3.30	±3.32	±4.90	±5.29	±4.02	±3.56	±5.46

Appendix C. Standard deviations of the residuals

Table C.1
Estimated median, minimum and maximum standard deviations (σ) of the residuals in North, East and up directions. The permanent GNSS stations SABY, SABA, SABN and SABP were computed with the Permanent Network (BSW-PN) processing strategy and the cost-effective units SC00-SC03 with the BSW-PN+CE processing strategy from Table 1. All values are indicated in mm.

	BSW-PN					BSW-PN+CE			
	Station	SABY	SABA	SABN	SABP	SC00	SC01	SC02	SC03
Parameter / # days		671	669	609	668	389	554	540	592
	Median σ	1.94	2.47	2.35	2.76	2.78	2.18	1.80	2.72
North	Min. σ	1.38	1.76	1.71	1.93	1.69	1.49	1.20	1.70
	Max. σ	3.18	4.15	4.41	3.86	3.69	3.41	2.61	3.74
	Median σ	1.82	4.07	3.50	4.76	3.72	2.03	2.79	4.85
East	Min. σ	1.25	2.75	2.44	3.36	2.19	1.37	1.90	3.08
	Max. σ	3.13	6.49	6.26	6.86	4.67	3.13	4.37	7.16
	Median σ	5.38	6.04	6.07	8.96	9.73	6.35	6.00	9.15
Up	Min. σ	3.64	4.24	4.25	6.21	5.47	4.29	4.06	5.65
	Max. σ	9.16	10.13	11.84	13.26	12.16	10.40	9.02	14.00

References

Anderson, K., Johanson, I., 2022. Incremental caldera collapse at kīlauea volcano recorded in ground tilt and high-rate gnss data, with implications for collapse dynamics and the magma system. Bull. Volcanol. 84, 89. https://doi.org/10.1007/s00445-022-01589-x.

Aoki, Y., 2024. Chapter 7 - measuring volcano deformation with gnss. In: Aoki, Y., Kreemer, C. (Eds.), GNSS Monitoring of the Terrestrial Environment. Elsevier, pp. 129–159. https://doi.org/10.1016/B978-0-323-95507-2.00016-5.

Banville, S., Hassen, E., Lamothe, P., Farinaccio, J., Donahue, B., Mireault, Y., Goudarzi, M.A., Collins, P., Ghoddousi-Fard, R., Kamali, O., 2021. Enabling ambiguity resolution in CSRS-PPP. NAVIGATION J. Inst. Navig. 68, 433–451.

Bevis, M., Businger, S., Herring, T.A., Rocken, C., Anthes, R.A., Ware, R.H., 1992. Gps meteorology: Remote sensing of atmospheric water vapor using the global positioning system. J. Geophys. Res. Atmos. 97, 15787–15801. https://doi.org/10.1029/92JD01517.

Blewitt, G., Lavallée, D., 2002. Effect of annual signals on geodetic velocity. Journal of Geophysical Research: Solid. Earth 107. https://doi.org/10.1029/2001JB000570. ETG 9–1–ETG 9–11.

Bonforte, A., Aiesi, G., Calvagna, F., Consoli, S., Pruiti, L., Rubonello, A., Saraceno, B., 2024. Real-time mobile GNSS network data acquired during the 2021–2022 unrest at Vulcano island. Bull. Volcanol. 86, 36. https://doi.org/10.1007/s00445-024-01711-1.

BRIGAID, 2020. Bridging the gap for innovations in disaster resilience. https://brigaid.eu. Accessed: 2024-06-13.

De Zeeuw-van Dalfsen, E., Sleeman, R., 2018. A permanent, real-time monitoring network for the volcanoes mount scenery and the Quill in the Caribbean Netherlands. Geosciences 8, 320.

Dumont, Q., Cayol, V., Froger, J.L., Peltier, A., 2022. 22 years of satellite imagery reveal a major destabilization structure at piton de la fournaise. Nat. Commun. 13, 2649.

Garrido-Carretero, M.S., Borque-Arancón, M.J., Ruiz-Armenteros, A.M., Moreno-Guerrero, R., Gil-Cruz, A.J., et al., 2019. Low-cost gnss receiver in rtk positioning under the standard iso-17123-8: a feasible option in geomatics. Measurement 137, 168–178.

Gili, J.A., Corominas, J., Rius, J., 2000. Using Global Positioning System techniques in landslide monitoring. Eng. Geol. 55, 167–192. https://doi.org/10.1016/S0013-7952(99)00127-1.

Hamza, V., Stopar, B., Sterle, O., 2021. Testing the performance of multi-frequency low-cost gnss receivers and antennas. Sensors 21, 2029.

Hohensinn, R., Stauffer, R., Glaner, M.F., Herrera Pinzón, I.D., Vuadens, E., Rossi, Y., Clinton, J., Rothacher, M., 2022. Low-cost gnss and real-time ppp: Assessing the precision of the u-blox zed-f9p for kinematic monitoring applications. Remote Sens. 14, 5100.

Jakowski, N., Heise, S., Wehrenpfennig, A., Schlüter, S., Reimer, R., 2002. Gps/glonass-based tec measurements as a contributor for space weather forecast. J. Atmos. Sol. Terr. Phys. 64, 729–735. https://doi.org/10.1016/S1364-6826(02)00034-2. Space Storms and Space Weather.

Janos, D., Kuras, P., Ortyl, L., 2022. FVconditions. Measurement 201, 111647.

Kreemer, C., Blewitt, G., Klein, E.C., 2014. A geodetic plate motion and global strain rate model. Geochem. Geophys. Geosyst. 15, 3849–3889. https://doi.org/10.1002/2014GC005407.

Krietemeyer, A., van Dalfsen, E., 2024. Cost-efficient gnss basestation sd card image for raspberry pi. https://doi.org/10.4121/65d51e7c-ea4c-40ce-9561-e556948b7a8a.

Krietemeyer, A., van der Marel, H., van de Giesen, N., ten Veldhuis, M.C., 2020. High quality zenith tropospheric delay estimation using a low-cost dual-frequency receiver and relative antenna calibration. Remote Sens. 12, 1393.

Krietemeyer, A., van der Marel, H., van de Giesen, N., Ten Veldhuis, M.C., 2022. A field calibration solution to achieve high-grade-level performance for low-cost dual-frequency gnss receiver and antennas. Sensors 22, 2267.

Leick, A., Rapoport, L., Tatarnikov, D., 2015. GPS Satellite Surveying. John Wiley & Sons, Hoboken, New Jersey.

Marut, G., Hadas, T., Nosek, J., 2024. Intercomparison of multi-gnss signals characteristics acquired by a low-cost receiver connected to various low-cost antennas. GPS Solutions 28, 82.

Nie, Z., Zhang, R., Liu, G., Jia, Z., Wang, D., Zhou, Y., Lin, M., 2016. Gnss seismometer: Seismic phase recognition of real-time high-rate gnss deformation waves. J. Appl. Geophys. 135, 328–337. https://doi.org/10.1016/j.jappgeo.2016.10.026 new trends in Induced Polarization.

Parks, M., Sigmundsson, F., Drouin, V., Hjartardóttir, Á.R., Geirsson, H., Hooper, A., Vogfjörd, K.S., Ófeigsson, B.G., Hreinsdóttir, S., Jensen, E.H., et al., 2023. Deformation, seismicity, and monitoring response preceding and during the 2022 fagradalsfjall eruption, Iceland. Bull. Volcanol. 85, 60.

Poland, M.P., de Zeeuw-van Dalfsen, E., 2021. Chapter 3 - Volcano geodesy: A critical tool for assessing the state of volcanoes and their potential for hazardous eruptive activity. In: Papale, P. (Ed.), Forecasting and Planning for Volcanic Hazards, Risks, and Disasters, Volume 2 of Hazards and Disasters Series. Elsevier, pp. 75–115. https://doi.org/10.1016/B978-0-12-818082-2.00003-2.

Poland, M.P., Peltier, A., Bonforte, A., Puglisi, G., 2017. The spectrum of persistent volcanic flank instability: a review and proposed framework based on kīlauea, piton de la fournaise, and Etna. J. Volcanol. Geotherm. Res. 339, 63–80. https://doi.org/10.1016/j.jvolgeores.2017.05.004.

Roobol, M., Smith, A., 2004. Volcanology of Saba and St. Eustatius, Northern Lesser Antilles. Koninklijke Nederlandse Akademie van Wetenschappen, Amsterdam, The Netherlands.

Saunders, S., Tenor, E., Wakawa, J., Nohou, J., 2023. Twenty-two years of GPS monitoring at Rabaul Caldera, a Narrative history. Geosciences 13. https://doi.org/10.3390/geosciences13080249.

Segall, P., Anderson, K.R., Johanson, I., Miklius, A., 2019. Mechanics of inflationary deformation during caldera collapse: evidence from the 2018 kīlauea eruption. Geophys. Res. Lett. 46, 11782–11789. https://doi.org/10.1029/2019GL084689.

Sleeman, R., de Zeeuw-van Dalfsen, E., 2022. Bridging the Seismic monitoring Gap around Saba, St. Eustatius, and St. Maarten in the Caribbean Netherlands: the NA Network. Bull. Seismol. Soc. Am. 113, 143–156. https://doi.org/10.1785/0120220126.

Takasu, T., 2013. RTKLIB: An Open Source Program Package for GNSS Positioning. URL. https://www.rtklib.com/prog/manual_2.4.2.pdf. version 2.4.2.

Teunissen, P., Montenbruck, O., 2017. Handbook of Global Navigation Satellite Systems. Springer, Berlin/Heidelberg, Germany.

Tunini, L., Zuliani, D., Magrin, A., 2022. Applicability of cost-effective gnss sensors for crustal deformation studies. Sensors 22, 350.

TWIGA, 2021. Transforming water, weather, and climate information through in situ observations for geo-services in africa. https://website.twiga-h2020.eu. Accessed: 2024-06-13.

Verweij, P., 2020. High precision positioning system for Ghana. URL. http://resolver.tudelft.nl/uuid:6c3ebc2c-b610-4a4d-950c-00058e27c1f6. Master Thesis Integrated Product Design.

Verweij, P., 2023. Low cost High Precision Positioning GNSS referencestation. https://github.com/PJ-Verweij/LowCostHighPrecisionPositioning-GNSSreferencestation.

Vidal, M., Jarrin, P., Rolland, L., Nocquet, J.M., Vergnolle, M., Sakic, P., 2024. Cost-Efficient Multi-GNSS Station with Real-Time Transmission for Geodynamics applications. Remote Sens. 16. https://doi.org/10.3390/rs16060991.

Widiwijayanti, C., Thin Zar Win, N., Espinosa-Ortega, T., Costa, F., Taisne, B., 2024. The global volcano monitoring infrastructure database (GVMID). Front. Earth Sci. 12, 1284889.

Wielgocka, N., Hadas, T., Kaczmarek, A., Marut, G., 2021. Feasibility of using low-cost dual-frequency gnss receivers for land surveying. Sensors 21, 1956.

Wilkinson, M.W., Bonforte, A., Jones, R.R., Wadsworth, F.B., Roberts, G.P., Guglielmino, F., 2023. The performance of differential point positioning using low-cost GNSS in comparison to DInSAR for monitoring coseismic displacement of the Provenzana–Pernicana fault system (Mt. Etna, 2018 December eruptive phase). Geophys. J. Int. 234, 1012–1023. https://doi.org/10.1093/gji/ggad118.

Zumberge, J.F., Heflin, M.B., Jefferson, D.C., Watkins, M.M., Webb, F.H., 1997. Precise point positioning for the efficient and robust analysis of gps data from large networks. J. Geophys. Res. Solid Earth 102, 5005–5017. https://doi.org/10.1029/96JB03860.